HHS Public Access

Author manuscript

Brain Stimul. Author manuscript; available in PMC 2025 May 28.

Published in final edited form as:

Brain Stimul. 2025 ; 18(3): 829–837. doi:10.1016/j.brs.2025.04.003.

Personalized models of Beam/F3 targeting in transcranial magnetic stimulation for depression: Implications for precision clinical translation

Divya Rajasekharan[a,b], **Michelle R. Madore**[a,b], **Paul Holtzheimer**[c,d], **Kelvin O. Lim**[e,f], **Leanne M. Williams**[a,b,1], **Noah S. Philip**[g,h,1,*]

[a]Department of Psychiatry and Behavioral Sciences, Stanford University School of Medicine, 401 Quarry Rd, Stanford, CA 94305, USA

[b]Mental Illness Research, Education and Clinical Center, VA Palo Alto Health Care System, 3801 Miranda Ave, Palo Alto, CA 94304, USA

[c]Geisel School of Medicine at Dartmouth, Hanover, NH, 03755, USA

[d]National Center for PTSD, VA Medical Center, U.S. Department of Veterans Affairs, 215 N Main St, White River Junction, VT 05009, USA

[e]Department of Psychiatry and Behavioral Sciences, University of Minnesota Medical School, Minneapolis, MN, 55455, USA

[f]Minneapolis VA Health Care System, 1 Veterans Drive, Minneapolis, MN 55417, USA

[g]Department of Psychiatry and Human Behavior, Alpert Medical School of Brown University, Providence, RI, 02903, USA

[h]Center for Neurorestoration and Neurotechnology, VA Providence Healthcare System, 830 Chalkstone Ave, Providence, RI 02908, USA

Abstract

Background: Clinical transcranial magnetic stimulation (TMS) for depression routinely relies on the scalp-based Beam/F3 targeting method to identify stimulation targets in the dorsolateral

[*]Corresponding author. Department of Psychiatry and Human Behavior, Alpert Medical School of Brown University, Providence, RI, 02903, USA. noah_philip@brown.edu (N.S. Philip).

[1]Equal senior authors.

CRediT authorship contribution statement

Divya Rajasekharan: Writing – review & editing, Writing – original draft, Visualization, Methodology, Formal analysis, Data curation, Conceptualization. **Michelle R. Madore:** Writing – review & editing, Supervision, Project administration, Funding acquisition, Data curation, Conceptualization. **Paul Holtzheimer:** Writing – review & editing, Supervision, Project administration, Funding acquisition. **Kelvin O. Lim:** Writing – review & editing, Supervision, Project administration, Funding acquisition. **Leanne M. Williams:** Writing – original draft, Supervision, Project administration, Funding acquisition, Data curation, Conceptualization. **Noah S. Philip:** Writing – review & editing, Writing – original draft, Supervision, Funding acquisition, Conceptualization.

Disclosures

The views expressed in this article are those of the authors and do not necessarily reflect the position or policy of the National Institutes of Health, National Science Foundation, or US Department of Veterans Affairs.

Appendix A. Supplementary data

Supplementary data to this article can be found online at https://doi.org/10.1016/j.brs.2025.04.003.

prefrontal cortex (dLPFC). Scalp-based targeting offers a low-cost and easily implemented method for TMS coil placement, enhancing treatment availability. However, limited anatomical and functional specificity of the Beam/F3 method may affect treatment outcomes, motivating assessment of the clinical standard.

Methods: In a naturalistic clinical trial of TMS conduced at four Veterans Affairs hospitals, the authors evaluate the Beam/F3 method using neuroimaging incorporated before TMS, after five treatment sessions, and after all thirty sessions. Personalized anatomical and electric field (E-field) models were developed to assess target location and network engagement, as well as subsequent effects on clinical outcomes.

Results: Anatomical models demonstrate that the Beam/F3 method produced reliable targets in the dLPFC across individuals and repeated treatment sessions. E-field models revealed that baseline anticorrelation between the stimulation center and the sgACC was associated with antidepressant symptom response after five TMS sessions ($p = 0.032$, $r^2 = 0.100$, $N = 46$) and at the end of treatment ($p = 0.042$, $r^2 = 0.107$, $N = 39$). Relatedly, E-field magnitude at the sgACC-anticorrelated peak in the prefrontal cortex correlated with symptom response throughout treatment (early treatment: $p = 0.001$, $r^2 = 0.220$, $N = 46$; end of treatment: $p = 0.026$, $r^2 = 0.127$, $N = 39$).

Conclusions: This work establishes that scalp-based targeting can produce reliable targets in the dLPFC and be successfully evaluated using a combination of neuroimaging and E-field modeling in pragmatic, multisite applications. Importantly, this investigation also found that significant network effects occur early in treatment and that Beam/F3 targets can engage functional mechanisms in TMS.

Keywords

TMS; Beam/F3; Depression; E-field; Modeling; dLPFC; sgACC

1. Introduction

Clinical transcranial magnetic stimulation (TMS) is an evidence-based treatment for pharmacoresistant depression [1–3]. In TMS, an electric coil is placed against the side of the head to noninvasively administer electromagnetic pulses to the brain through the skull. TMS electric fields effectively stimulate activity in cortical neurons, achieving both acute and long-term neuroplastic effects in the brain [4–8].

Most commonly, TMS is applied to the dorsolateral prefrontal cortex (dLPFC) to treat depression. The dLPFC comprises a relatively large region of the prefrontal cortex, and the task of targeting precise anatomical and functional sites to optimize clinical outcomes remains a pressing challenge [9–12]. Since the Food and Drug Administration's original clearance of TMS for depression in 2008, several studies have demonstrated that symptom improvement relates to both the anatomical location as well as the functional network relationships of the TMS target site. These findings have driven the development of increasingly precise and personalized TMS targeting strategies [13–19], but clinical practice continues to primarily rely on scalp-based coil placement.

The most prevalent scalp-based targeting method is the modified Beam/F3 technique, adapted from the 10–20 system for the placement of EEG electrodes. In this method, personalized skull measurements are used to place the TMS coil above the stereographic F3 site, which corresponds to the dLPFC in most individuals [20,21]. Variability in patient anatomy drives differences in the exact cortical targets that are achieved using scalp-based heuristics [21–24]. The correspondence of Beam/F3 targets to individual brain anatomy and subject-specific functional organization of the cortex likely influences TMS efficacy in clinical settings [8,25]. There is an urgent need to systematically evaluate the precision of scalp-based targeting and its ability to engage mechanisms of antidepressant response in clinical TMS.

TMS induces a distributed electrical signal over the cortical surface, which further complicates the assessment of TMS targets [26,27]. Previous studies have assumed that the focal point of stimulation lies directly below the coil center, but whether this assumption is valid remains unclear. Personalized electric field (E-field) models offer the advantage of estimating a continuous distribution of stimulated tissue based on physical laws of electromagnetic induction. Typically, the use of these models has been restricted to research settings, particularly those equipped to record coil position in real time using frameless stereotaxy. Adapting E-field modeling for clinical TMS offers a unique opportunity to characterize the brain areas that are stimulated by scalp-based targeting.

The correspondence of E-fields induced by scalp-based targeting to potential resting state network mechanisms in TMS may provide insight into factors determining clinical outcome [4,8,25,28]. Several studies have demonstrated that stronger anticorrelation between the stimulation target and the subgenual anterior cingulate cortex (sgACC) is associated with symptom response, suggesting the presence of a dLPFC-sgACC functional brain axis that can be therapeutically modulated using TMS. Although these studies report a range of effect sizes ($.003 \leq r^2 \leq .28$), they nevertheless provide a framework to systematically evaluate the extent to which Beam/F3 stimulation engages functional mechanisms relevant to treatment outcome [29–32].

Here, we present a model-driven investigation of the scalp-based, modified Beam/F3 targeting method (hereafter referred to simply as Beam/F3) used to deliver TMS in clinical settings at four Veterans Affairs (VA) hospitals. Data were acquired as part of the pragmatic B-SMART-fMRI trial, which implements magnetic resonance imaging (MRI) during a routine course of clinical TMS [33]. Imaging was acquired before treatment, after five sessions, and after all 30 sessions. To start, we reconstructed 3D anatomical models from structural MRI to assess the precision of Beam/F3 targets across subjects and repeated treatment sessions. Next, we developed personalized E-field models by combining subject-specific anatomical models with individualized coil placement and stimulation parameters. The magnitude of the TMS E-field was analyzed to characterize the spatial distribution of the stimulation produced by Beam/F3 targeting. Lastly, we integrated resting state functional MRI (fMRI) to evaluate whether Beam/F3 stimulation effectively engaged baseline neural connectivity mechanisms of antidepressant response. Specifically, we tested whether pretreatment functional connectivity between Beam/F3 stimulation sites and the sgACC was associated with symptom reduction, hypothesizing that E-field models would

more robustly reveal a relationship between functional sgACC engagement and treatment outcome when compared to anatomical models alone.

2. Methods

2.1. Study Design

As part of the parent B-SMART-fMRI trial (NCT04663481), veterans with treatment-resistant depression were recruited from four sites participating in the VA Clinical TMS Program [34]. As part of the VA program, veterans receive thirty sessions of daily 10 Hz TMS. Study participants additionally underwent structural and functional MRI at three timepoints: before the start of treatment (Baseline), after the first five TMS sessions (Early Treatment), and after thirty sessions (Post Treatment). Symptom severity was assessed at each timepoint using self-reported questionnaires. VA sites (and academic partners for MRI data collection) are the Palo Alto VA (Stanford University), the Minneapolis VA (University of Minnesota), the Providence VA (Brown University), and the White River Junction VA (Dartmouth College). The parent trial includes additional endpoint measures, a planned interim analysis [35], and a planned evaluation of the Beam/F3 method, which is the focus of the present analysis.

2.2. Sample

Participants met DSM-5 MDD criteria and qualified as treatment-resistant by failing to respond to at least one prior, adequate antidepressant trial. Standard exclusion criteria for TMS were applied, and subjects were required to meet criteria for MRI compatibility. Subjects maintained preestablished medication regimens throughout study involvement. For details, refer to the published protocol paper [33].

Participants provided informed, written consent in accordance with site Institutional Review Boards. By December 1st, 2023, n = 50 participants were enrolled in standard TMS across the four sites. Specific criteria for inclusion in the present analysis were collection of pretreatment resting state fMRI and at least one follow-up assessment of symptom severity. Additionally, one participant was excluded due to poor structural image quality, which prevented accurate segmentation and modeling. Per these criteria, n = 46 participants were eligible for analysis at the Early Treatment timepoint, and n = 39 participants were retained Post Treatment. See Supplementary Material for CONSORT diagram (Fig. S1). Sample demographics were representative of VA patients (Table 1).

2.3. Beam/F3 measurement

At a pretreatment visit, the principal TMS administrator at each site applied the modified Beam/F3 method to identify the Beam/F3 scalp target on a sized TMS cap. The nasion-to-inion distance, tragus-to-tragus distance, and head circumference were recorded in centimeters using a tape measure [20]. Measurements were inputted into the modified Beam/F3 algorithm, accessed through a web-based interface [36]. The outputted X and “Adjusted” Y coordinates were used to locate the Beam/F3 target on the scalp [21]. Clinicians participating in the VA Clinical TMS Program undergo standardized training

consisting of both online modules and an in-person skills development workshop at the Palo Alto VA, supervised by co-author MRM and partly instructed by co-author NSP.

2.4. TMS protocol

During treatment, the coil was centered on the Beam/F3 target and placed parallel to the scalp, with the coil handle oriented 45° away from the midsagittal plane. Stimulation intensity was prescribed at 120% of the subject's pretreatment motor threshold; occasionally, operators reduced intensity if the subject had difficulty tolerating stimulation. In each session, a repetitive TMS (rTMS) protocol consisting of 3000 pulses was administered in the form of 75 trains delivering 40 pulses at a frequency of 10 Hz. Trains were separated by an inter-stimulus interval of 11–26 s. Over the course of six weeks, participants received treatment once a day for five days a week, resulting in thirty total sessions.

2.5. Neuroimaging

2.5.1. Structural scans: Participants underwent MRI at three distinct timepoints (i.e., Baseline, Early Treatment, and Post Treatment), as previously described. At each timepoint, a T1-weighted structural scan was acquired with a 0.8 mm isotropic voxel, 320 axial slices, 224 × 320 acquisition matrix, TE of 3.77 ms, TR of 2.84 s, and flip angle of 8°. Importantly, each subject wore their TMS cap into the scanner with a high-contrast gel capsule attached to the Beam/F3 target.

2.5.2. Functional scans: Resting state fMRI was collected at each timepoint using a multiband acquisition scheme. A total of 60 axial slices were acquired per volume with a 2.4 mm isotropic voxel, 90 × 90 acquisition matrix, TE of 3.1 ms, TR of 710 ms, flip angle of 54°, and multiband factor of 6. Data collection was divided into two sequences lasting 7.90 min each with opposite phase-encoding directions. Field maps were collected at each session. Resting state fMRI data was preprocessed using fMRIPrep for motion and slice-time correction, as well as susceptibility distortion correction using field maps [37]. XCP-D was applied for global signal regression, regression of motion and non-gray matter signal confounds, and spatial smoothing using a 6 mm FWHM Gaussian kernel [38].

2.5.3. sgACC definition: A sgACC mask was defined as previously described in the work of co-author LMW [39]. In brief, a search for the term "threat" was conducted in the meta-analytic database, Neurosynth [40]. Peak coordinates were identified for clusters surviving false discovery rate correction ($p < 0.01$). A sgACC peak was identified at $x = 4$, $y = 26$, and $z = -10$ in MNI space, and an ROI was defined to contain all neighboring voxels within 10 mm.

2.6. Clinical measures

Clinical depression severity was evaluated at each timepoint using the Quick Inventory of Depressive Symptomatology questionnaire via self-report (QIDS-SR) [41].

2.7. Anatomical modeling

To localize the Beam/F3 scalp target to the cortical surface and perform E-field modeling, we generated 3D anatomical models from structural MRI for each participant in subject

space. Cortical targets were subsequently mapped to the volumetric MNI template and the surface-based Glasser atlas for group-level analysis and comparison. For additional details, see Supplementary Material.

2.7.1. Constructing head models: Structural scans from each timepoint were averaged into a single, denoised image using fMRIPrep. Then, we applied the FreeSurfer *recon-all* tool to perform automated, surface-driven segmentation of the brain tissue [42]. The surrounding cerebrospinal fluid, meninges, skull, and scalp were segmented using the *CHARM* tool, distributed as part of SimNIBS 4.0 [43]. We combined the results from the two segmentation tools into a single multi-label segmentation, delineating a total of 8 tissue classes: gray matter (GM), white matter (WM), cerebrospinal fluid (CSF), blood, compact bone, spongy bone, eyeballs, and skin. For each subject, we spent an average of 4–6 h manually correcting segmentation errors at the CSF-skull boundary near the prefrontal cortex, given its proximity to the TMS coil. All corrections were performed by first author DR and checked by senior author NSP. Lastly, *CHARM* was used to convert the segmented image volume into a finite element mesh consisting of linear tetrahedral elements.

2.7.2. Reconstructing TMS targets: We recorded the coordinates of the center of the gel capsule in all available structural images. In the anatomical model, the closest scalp vertex to the capsule was identified as the Beam/F3 scalp target in subject space. The scalp target was projected orthogonally across the scalp (i.e., parallel to the coil axis) onto the cortex to generate a Beam/F3 cortical target in subject space.

2.7.3. Transforming Beam/F3 targets to template spaces: For each participant, the Beam/F3 cortical target in subject space was transformed to the volumetric MNI template for functional connectivity analysis and the surface-based Glasser atlas for anatomical classification [44].

2.8. E-field modeling

For each subject, we used SimNIBS 4.0 to simulate the maximum E-field induced during a single pulse of rTMS [45].

2.8.1. Coil position: A separate simulation was run for each imaging timepoint, approximating the E-field distribution at the preceding treatment session. The center of the TMS coil in simulation was placed at the location of the Beam/F3 scalp target, derived from the gel capsule position in the corresponding session image.

2.8.2. Coil orientation: We modeled the coil orientation using a series of geometric calculations, dictated by the clinical positioning guidelines. Using the reconstructed anatomical surfaces, we identified the tangent plane to the scalp at the Beam/F3 target and labeled its outward unit normal $\hat{n}$. Then, we projected the posterior-to-anterior axis (denoted $\hat{v}$) onto the tangent plane, or

$$\overrightarrow{v}_{\parallel} = \hat{v} - (\hat{v} \cdot \hat{n})\hat{n}\,.$$

Finally, we rotated the vector $\hat{v}_{\parallel} = \overrightarrow{v}_{\parallel} / |\overrightarrow{v}_{\parallel}|$ 45° clockwise in-plane to estimate the direction of the coil handle, $\hat{w}$, as

$$\hat{w} = \frac{\hat{v}_{\parallel}}{\sqrt{2}} - \frac{\hat{n} \times \hat{v}_{\parallel}}{\sqrt{2}}.$$

2.8.3. Stimulation parameters: The maximum slope of the TMS current pulse, $\frac{dI^*}{dt}$, was approximated from the prescribed stimulation intensity for each individual and used to parameterize the E-field simulation (for details, see Supplementary Material).

2.8.4. Simulating electric fields: Using SimNIBS, the E-fields induced by TMS were numerically approximated by assuming linear conducting materials and quasi-magnetostatic fields. Given the dosing parameter $\frac{dI^*}{dt}$ and a model of the coil [46], SimNIBS computes the time derivative of the magnetic vector potential, $\partial_t \overrightarrow{A}$, which acts as a forcing function in the quasi-magnetostatic formulation of Maxwell's equations [53], or

$$\overrightarrow{\nabla} \cdot \left[\sigma \left(\overrightarrow{\nabla} \boldsymbol{\Phi} - \partial_t \overrightarrow{A} \right) \right] = 0.$$

Here, σ is the tissue electrical conductivity and Φ is a scalar potential field. The scalar potential at each node in the mesh is solved using the finite element method, allowing the E-field vector to be inferred at each node as

$$\overrightarrow{\mathrm{E}} = \overrightarrow{\nabla} \boldsymbol{\Phi} - \partial_t \overrightarrow{A}.$$

We used the default scalar isotropic electrical conductivities available in simNIBS for each tissue class.

2.9. Analysis

2.9.1. Precision across treatment sessions: The precision of Beam/F3 targets across treatment sessions was quantified as the root-mean-square (RMS) distance of the session targets ($\langle x_s, y_s, z_s \rangle$) to the average target ($\langle \bar{x}, \bar{y}, \bar{z} \rangle$), or

$$\sqrt{\frac{1}{|S|} \sum_{s \in S} (x_s - \bar{x})^2 + (y_s - \bar{y})^2 + (z_s - \bar{z})^2},$$

where S denotes the set of all available images with a visible gel capsule attached to the Beam/F3 target.

2.9.2. E-field magnitude and overlap in the dLPFC: The dLPFC was defined according to the Glasser atlas, comprising areas 8C_L, 8Av_L, i6–8_L, s6–8_L, SFL_L, 8BL_L, 9p_L, 9a_L, 8Ad_L, p9–46v_L, a9–46v_L, 46_L, and 9–46d_L. We calculated the mean E-field in the dLPFC as well as the overlap between the dLPFC and the electrically

stimulated region. We defined a mask V containing cortical voxels stimulated at ≥95th percentile of the cortical E-field and computed its intersection with the dLPFC mask D as

$$\frac{|V \cap D|}{|D|}.$$

2.9.3. Effect of pretreatment target-sgACC anticorrelation on treatment outcome: To assess target-sgACC anticorrelation, we considered two methods for identifying the locus of TMS stimulation. As previously described, the Beam/F3 scalp target was projected onto the cortical surface to render a first-order estimate. To incorporate insights about the distribution of the stimulus from E-field simulations, we used the previously defined E-field 95th percentile mask, V, to identify the E-field center of gravity (CoG), calculated as the weighted average cortical position of all voxels v_i within this mask,

$$\overrightarrow{CoG} = \frac{\sum_{v_i \in V} \vec{r}_i \left|\vec{E}_i\right|}{\sum_{v_i \in V} \left|\vec{E}_i\right|}.$$

To evaluate baseline functional connectivity (FC) between the TMS stimulation site and the subgenual anterior cingulate cortex (sgACC), we quantified the Pearson's r correlation between the resting state BOLD time series in the sgACC and 1) the projected Beam/F3 cortical target, and 2) the E-field CoG. We analyzed the association between the two pretreatment FC measures and the percent change in QIDS-SR score after Early Treatment and Post Treatment, compared to Baseline.

2.9.4. Effect of E-field magnitude at prefrontal sgACC-anticorrelated peak on treatment outcome: To investigate the possibility that sgACC functional engagement and associated antidepressant mechanisms in TMS are related to stimulation of an 'optimal' functional target, as previously suggested [10,29], we identified the voxel that was maximally anticorrelated to the sgACC in the prefrontal cortex and averaged its location across timepoints (for details, see Supplementary Material). We tested the association between the average simulated E-field magnitude at the sgACC-anticorrelated peak and symptom improvement after Early Treatment and Post Treatment.

3. Results

3.1. Precision of Beam/F3 targets

3.1.1. Precision across subjects: Personalized anatomical models were constructed from structural MRI for each participant. Using the gel capsule marker, the position of the scalp target was assessed relative to patient brain anatomy (Fig. 1a). A cortical target was derived by projecting the scalp target orthogonally onto the brain (Fig. 1b). The average [±SD] projected cortical target was located at $x = -40$ [±5.0] mm, $y = 34$ [±10] mm, and $z = 41$ [±7.8] mm in MNI space (Fig. 1c). Across participants, the mean distance to the average target was 1.2 cm. In the Glasser atlas, targets primarily fell into Areas 46 [41 %], 8Av [24 %], 9–46d [9 %], 9–46v [9 %], 8C [4 %] and 8Ad [4 %]. Areas 9a, 9p, IFSp, and i6–8L

each contained targets for one participant. Targets corresponded to the dLPFC for 98 % of participants (Fig. 1d).

3.1.2. Precision across treatment sessions: With imaging acquired at up to three timepoints throughout TMS, variability in the gel capsule position across images was used to approximate the inter-session targeting precision of the Beam/F3 method. The median (IQR) precision was 5.0 (4.3) mm for scalp targets and 4.6 (4.2) mm for projected cortical targets (Fig. 1e and f).

3.2. E-fields induced by Beam/F3 targets

E-field models were generated for each participant using SimNIBS 4.0. Exemplary E-field distributions corresponding to the 95th percentile and above are demonstrated for a single subject from each site (Fig. 2). The 95th percentile of the cortical E-field reliably overlapped with the dLPFC across subjects, ranging from 45.9% at minimum to 78.6% at maximum. The mean [±SD] overlap was 68.6% [±7.4%]. The average E-field magnitude in the dLPFC was 184 [±57] V/m.

It was evident from simulation that the E-field distribution induced by TMS was not symmetric nor centered on the cortical target, as commonly assumed. Instead, the median (IQR) distance between the cortical target and the E-field center of gravity was 14.4 (5.0) mm. The peak of the E-field distribution aligned somewhat more closely with the cortical target, with a median separation of 9.6 (7.7) mm across subjects. While local maxima in the E-field distribution occurred at gyral crowns near the cortical target, the ellipsoidal shape and inclination of the brain caused the E-field to propagate posteroinferiorly.

3.3. E-field relationships with treatment outcome

Lastly, we evaluated whether clinical TMS efficacy was associated with target engagement of sgACC anticorrelation in the prefrontal cortex, as previously reported [29,31,32]. We used three distinct metrics—sgACC anticorrelation of the projected Beam/F3 target, sgACC anticorrelation of the E-field center of gravity, and E-field magnitude at the sgACC-anticorrelated peak in the prefrontal cortex—to assess a potential relationship between TMS stimulation of sgACC-linked functional nodes and clinical outcome.

3.3.1. Effect of pretreatment target-sgACC anticorrelation on treatment outcome: We used two methods to estimate the locus of functional stimulation in the dLPFC—the projected Beam/F3 target and the E-field CoG—and tested whether baseline anticorrelation between these nodes and the sgACC was associated with treatment outcome (Fig. 3). When incorporating the E-field, we found that stronger baseline anticorrelation between the E-field CoG and the sgACC was positively correlated with symptom improvement (e.g., percent reduction in QIDS-SR score). This relationship was significant after five sessions ($p = 0.032$, $r^2 = 0.100$, $N = 46$) and at the end of treatment ($p = 0.042$, $r^2 = 0.107$, $N = 40$). Interestingly, without the E-field data, there were no significant associations between baseline target-sgACC connectivity and antidepressant outcomes (after five sessions: $p = 0.716$, $r^2 = 0.003$, $N = 46$; end of treatment : $p = 0.877$, $r^2 = 0.001$, $N = 39$).

3.3.2. Effect of E-field magnitude at prefrontal sgACC-anticorrelated peak on treatment outcome: Next, we considered the magnitude of E-field stimulation at the peak sgACC-anticorrelated node in the prefrontal cortex (Fig. 4). Since prior studies have reported fluctuation in coordinates derived from sgACC connectivity over time [47], we averaged the location of this node across timepoints to render a more reliable estimate. Using this approach, we found that the magnitude of the E-field at the sgACC-anticorrelated peak was associated with symptom improvement after both five sessions ($p = 0.001$, $r^2 = 0.220$, $N = 46$) and at the end of treatment ($p = 0.026$, $r^2 = 0.127$, $N = 39$). This relationship was still significant when the E-field magnitude was normalized with respect to the maximum cortical E-field for each subject (after five sessions: $p = 0.028$, $r^2 = 0.105$, $N = 46$; end of treatment: $p = 0.040$, $r^2 = 0.109$, $N = 39$).

4. Discussion

TMS is a necessary treatment option for individuals with major depressive disorder who do not respond to first-line treatments. Expanding access to TMS requires methods that are both cost effective and scalable. Targeting strategies like the Beam/F3 method meet these requirements, but whether they achieve the level of personalization needed to engage functional mechanisms in TMS remains unclear. Currently, clinical response rates can fall below 50%, indicating a pressing need to optimize protocols [48–50]. The effort to improve TMS outcomes requires a rigorous evaluation of the clinical standard of scalp-based targeting and its ability to effectively exploit neural mechanisms of response [18,28,51,52].

Our investigation of the Beam/F3 method revealed that targets primarily fall within the dLPFC. This method enabled consistent placement of the TMS coil across sessions and individuals, independent of the TMS operator or treatment center. The nationwide VA Clinical TMS Program implements a uniform training program for all clinicians, which we consider essential to the reliability of Beam/F3 targets observed in this multi-site study.

To our knowledge, E-field modeling has not been extensively applied to clinical TMS, partly due to methodological constraints. Using our model-based approach, we demonstrate that the top 95th percentile of the E-field induced by Beam/F3 targeting consistently coincides with the dLPFC, whether the coil was centered directly above the dLPFC or not. The clinical impact of E-field focality in the dLPFC is an important question for future study. Our results indicate that the Beam/F3 method targets multiple brain regions within the Glasser atlas, distinguished by their functional network associations. Whether this variation affects symptoms modulated by TMS depends on whether the corresponding E-field distributions have a normalizing or differentiating effect on network engagement.

Our findings in clinical TMS confirm prior reports that sgACC functional engagement is associated with treatment outcome. In this cohort, an effect was not isolated when examining the cortical target alone. Instead, several properties of the E-field distribution were needed to illustrate the effect of sgACC-linked functional pathways on clinical improvement. First, the extent to which the E-field center of gravity was functionally anticorrelated with the sgACC at baseline was associated with treatment outcome. Second, the magnitude of the E-field at the time-averaged sgACC-anticorrelated peak in the prefrontal cortex was correlated

with symptom reduction. These findings indicate that representing TMS stimulation by a single point is insufficient—distributed E-field properties conjunctly influence the network mechanisms engaged by TMS. Future optimization of the Beam/F3 targeting approach should incorporate E-field modeling and is an anticipated future direction for the current study.

The effect of sgACC functional engagement on symptom outcome emerged within five TMS sessions, highlighting a potential early response biomarker. While scalp-based heuristics may not optimize network engagement, they can serve as a first-line approach to identify responders early in treatment. Personalized functional targeting can be employed when scalp-based heuristics fail to provoke an early response, aligned with a measurement-based approach to care. Applying these techniques in tandem allows us to balance accessibility and precision, paving the path forward for TMS as an effective depression treatment.

The present analysis is subject to limitations, including a modest sample size. Prospective validation in larger cohorts is needed to confirm the importance of sgACC target engagement to TMS response, particularly early in treatment. Additionally, we have only considered the overall magnitude of the E-field in characterizing its effect on treatment outcome—in practice, several physical factors, including the direction of the E-field vector and the pattern of induced currents, may determine neural activity within the dLPFC and downstream effects on distal brain regions. Methodologically, the validity of our findings is constrained by the accuracy of our models: MRI-based anatomical models are always subject to improvement, and brain tissue electrical properties require further measurement to capture anisotropy and individual variability. Despite these limitations, TMS models provide critical insights into treatment mechanism. With continued refinement and validation, simulation techniques for TMS have the potential to inform treatment protocols, including scalp-based targeting, enhancing treatment outcomes and accessibility.

5. Conclusion

This work demonstrates that the modified Beam/F3 technique is a reliable method with a sound neuroanatomical basis. These findings also provide a benchmark for comparison to TMS trials using neuronavigation or personalized functional targeting. Previous studies have provided mixed evidence for the role of target-sgACC anticorrelation in antidepressant outcome, typically using anatomical points to represent the stimulation site. This investigation clarifies that TMS-induced E-field distributions may be required to explain sgACC engagement and its related antidepressant effect. Furthermore, the clinical impact of sgACC mechanisms emerged within five TMS sessions, providing a basis for an early response biomarker.

Supplementary Material

Refer to Web version on PubMed Central for supplementary material.

Acknowledgements

This study is funded by the National Institute of Mental Health (NIMH), grant number R01MH120126, awarded to co-authors LMW, MRM, KOL, NSP and PH. First author DR is supported by the National Science Foundation (NSF) Graduate Research Fellowship and the Stanford Bio-X PhD Fellowship. Kristoffer Madsen developed the custom Magstim E-z Cool Coil model used in this study. We extend our appreciation to Axel Thielscher, Oula Puonti, and the entire SimNIBS team for their help. Effort for this study at VA Providence is provided by the Center for Neurorestoration and Neurotechnology (I50 RX002864). We thank all our participants.

Declaration of competing interest

The authors declare the following financial interests/personal relationships which may be considered as potential competing interests: Leanne M. Williams reports financial support was provided by National Institute of Mental Health. Noah S. Philip reports a relationship with Neurolief that includes: funding grants. Noah S. Philip reports a relationship with Wave Neuroscience LLC that includes: funding grants. Noah S. Philip reports a relationship with Pulvinar Neuro that includes: board membership and consulting or advisory. Noah S. Philip reports a relationship with Motif Neurotech that includes: consulting or advisory. Leanne M. Williams reports a relationship with Laureate Institute for Brain Research that includes: board membership and consulting or advisory. Leanne M. Williams has patent #16921388 issued to Et Cere Inc. Paul Holtzheimer receives royalties from UpToDate and the Oxford University Press. If there are other authors, they declare that they have no known competing financial interests or personal relationships that could have appeared to influence the work reported in this paper.

References

[1]. Dalhuisen I, Van Oostrom I, Spijker J, Wijnen B, Van Exel E, Van Mierlo H, et al. rTMS as a next step in antidepressant nonresponders: a randomized comparison with current antidepressant treatment approaches. Am J Psychiatr 2024: 20230556. 10.1176/appi.ajp.20230556. appi.ajp.

[2]. Brunoni AR, Chaimani A, Moffa AH, Razza LB, Gattaz WF, Daskalakis ZJ, et al. Repetitive transcranial magnetic stimulation for the acute treatment of major depressive episodes: a systematic review with network meta-analysis. JAMA Psychiatry 2017;74:143. 10.1001/jamapsychiatry.2016.3644. [PubMed: 28030740]

[3]. Carpenter LL, Janicak PG, Aaronson ST, Boyadjis T, Brock DG, Cook IA, et al. Transcranial magnetic stimulation (TMS) for major depression: a multisite, naturalistic, observational study of acute treatment outcomes in clinical practice. Depress Anxiety 2012;29:587–96. 10.1002/da.21969. [PubMed: 22689344]

[4]. Liston C, Chen AC, Zebley BD, Drysdale AT, Gordon R, Leuchter B, et al. Default mode network mechanisms of transcranial magnetic stimulation in depression. Biol Psychiatry 2014;76:517–26. 10.1016/j.biopsych.2014.01.023. [PubMed: 24629537]

[5]. Ge R, Humaira A, Gregory E, Alamian G, MacMillan EL, Barlow L, et al. Predictive value of acute neuroplastic response to rTMS in treatment outcome in depression: a concurrent TMS-fMRI trial. Am J Psychiatr 2022;179:500–8. 10.1176/appi.ajp.21050541. [PubMed: 35582784]

[6]. Li X, Nahas Z, Kozel FA, Anderson B, Bohning DE, George MS. Acute left prefrontal transcranial magnetic stimulation in depressed patients is associated with immediately increased activity in prefrontal cortical as well as subcortical regions. Biol Psychiatry 2004;55:882–90. 10.1016/j.biopsych.2004.01.017. [PubMed: 15110731]

[7]. Nestor SM, Mir-Moghtadaei A, Vila-Rodriguez F, Giacobbe P, Daskalakis ZJ, Blumberger DM, et al. Large-scale structural network change correlates with clinical response to rTMS in depression. Neuropsychopharmacology 2022;47: 1096–105. 10.1038/s41386-021-01256-3. [PubMed: 35110687]

[8]. Philip NS, Barredo J, Aiken E, Carpenter LL. Neuroimaging mechanisms of therapeutic transcranial magnetic stimulation for major depressive disorder. Biol Psychiatry Cogn Neurosci Neuroimaging 2018;3:211–22. 10.1016/j.bpsc.2017.10.007. [PubMed: 29486862]

[9]. Herbsman T, Avery D, Ramsey D, Holtzheimer P, Wadjik C, Hardaway F, et al. More lateral and anterior prefrontal coil location is associated with better repetitive transcranial magnetic stimulation antidepressant response. Biol Psychiatry 2009;66:509–15. 10.1016/j.biopsych.2009.04.034. [PubMed: 19545855]

[10]. Cash RFH, Cocchi L, Lv J, Fitzgerald PB, Zalesky A. Functional magnetic resonance imaging–guided personalization of transcranial magnetic stimulation treatment for depression. JAMA Psychiatry 2021;78:337. 10.1001/jamapsychiatry.2020.3794. [PubMed: 33237320]

[11]. Fitzgerald PB, Hoy K, McQueen S, Maller JJ, Herring S, Segrave R, et al. A randomized trial of rTMS targeted with MRI based neuro-navigation in treatment-resistant depression n.d.

[12]. Herwig U, Padberg F, Unger J, Spitzer M, Schönfeldt-Lecuona C. Transcranial magnetic stimulation in therapy studies: examination of the reliability of "standard" coil positioning by neuronavigation. Biol Psychiatry 2001;50:58–61. 10.1016/S0006-3223(01)01153-2. [PubMed: 11457424]

[13]. Luber BM, Davis S, Bernhardt E, Neacsiu A, Kwapil L, Lisanby SH, et al. Using neuroimaging to individualize TMS treatment for depression: toward a new paradigm for imaging-guided intervention. Neuroimage 2017;148:1–7. 10.1016/j.neuroimage.2016.12.083. [PubMed: 28062252]

[14]. Cash RFH, Weigand A, Zalesky A, Siddiqi SH, Downar J, Fitzgerald PB, et al. Using brain imaging to improve spatial targeting of transcranial magnetic stimulation for depression. Biol Psychiatry 2021;90:689–700. 10.1016/j.biopsych.2020.05.033. [PubMed: 32800379]

[15]. Cole EJ, Stimpson KH, Bentzley BS, Gulser M, Cherian K, Tischler C, et al. Stanford accelerated intelligent neuromodulation therapy for treatment-resistant depression. Am J Psychiatr 2020;177:716–26. 10.1176/appi.ajp.2019.19070720. [PubMed: 32252538]

[16]. Gogulski J, Ross JM, Talbot A, Cline CC, Donati FL, Munot S, et al. Personalized repetitive transcranial magnetic stimulation for depression. Biol Psychiatry Cogn Neurosci Neuroimaging 2023;8:351–60. 10.1016/j.bpsc.2022.10.006. [PubMed: 36792455]

[17]. Siddiqi SH, Taylor SF, Cooke D, Pascual-Leone A, George MS, Fox MD. Distinct symptom-specific treatment targets for circuit-based neuromodulation. Am J Psychiatr 2020;177:435–46. 10.1176/appi.ajp.2019.19090915. [PubMed: 32160765]

[18]. Cocchi L, Zalesky A. Personalized transcranial magnetic stimulation in psychiatry. Biol Psychiatry Cogn Neurosci Neuroimaging 2018;3:731–41. 10.1016/j.bpsc.2018.01.008. [PubMed: 29571586]

[19]. Fox MD, Liu H, Pascual-Leone A. Identification of reproducible individualized targets for treatment of depression with TMS based on intrinsic connectivity. Neuroimage 2013;66:151–60. 10.1016/j.neuroimage.2012.10.082. [PubMed: 23142067]

[20]. Beam W, Borckardt JJ, Reeves ST, George MS. An efficient and accurate new method for locating the F3 position for prefrontal TMS applications. Brain Stimul 2009;2:50–4. 10.1016/j.brs.2008.09.006. [PubMed: 20539835]

[21]. Mir-Moghtadaei A, Caballero R, Fried P, Fox MD, Lee K, Giacobbe P, et al. Concordance between BeamF3 and MRI-neuronavigated target sites for repetitive transcranial magnetic stimulation of the left dorsolateral prefrontal cortex. Brain Stimul 2015;8:965–73. 10.1016/j.brs.2015.05.008. [PubMed: 26115776]

[22]. Herwig U, Satrapi P, Schönfeldt-Lecuona C. Using the international 10–20 EEG system for positioning of transcranial magnetic stimulation. Brain Topogr 2003;16: 95–9. 10.1023/B:BRAT.0000006333.93597.9d. [PubMed: 14977202]

[23]. Fabregat-Sanjuan A, Pámies-Vilá R, Pascual-Rubio V. Evaluation of the Beam-F3 method for locating the F3 position from the 10–20 international system. Brain Stimul 2022;15:1011–2. 10.1016/j.brs.2022.07.002. [PubMed: 35863653]

[24]. Trapp NT, Bruss J, King Johnson M, Uitermarkt BD, Garrett L, Heinzerling A, et al. Reliability of targeting methods in TMS for depression: beam F3 vs. 5.5 cm. Brain Stimul 2020;13:578–81. 10.1016/j.brs.2020.01.010. [PubMed: 32289680]

[25]. Fox MD, Buckner RL, Liu H, Chakravarty MM, Lozano AM, Pascual-Leone A. Resting-state networks link invasive and noninvasive brain stimulation across diverse psychiatric and neurological diseases. Proc Natl Acad Sci 2014;111. 10.1073/pnas.1405003111. [PubMed: 24324143]

[26]. Opitz A, Windhoff M, Heidemann RM, Turner R, Thielscher A. How the brain tissue shapes the electric field induced by transcranial magnetic stimulation. Neuroimage 2011;58:849–59. 10.1016/j.neuroimage.2011.06.069. [PubMed: 21749927]

[27]. Thielscher A, Opitz A, Windhoff M. Impact of the gyral geometry on the electric field induced by transcranial magnetic stimulation. Neuroimage 2011;54:234–43. 10.1016/j.neuroimage.2010.07.061. [PubMed: 20682353]

[28]. Holtzheimer PE. Defining mechanisms of transcranial magnetic stimulation as a treatment for depression through neuroimaging: progress and challenges. Biol Psychiatry Cogn Neurosci Neuroimaging 2018;3:201–2. 10.1016/j.bpsc.2018.01.011. [PubMed: 29486857]

[29]. Weigand A, Horn A, Caballero R, Cooke D, Stern AP, Taylor SF, et al. Prospective validation that subgenual connectivity predicts antidepressant efficacy of transcranial magnetic stimulation sites. Biol Psychiatry 2018;84:28–37. 10.1016/j.biopsych.2017.10.028. [PubMed: 29274805]

[30]. Elbau IG, Lynch CJ, Downar J, Vila-Rodriguez F, Power JD, Solomonov N, et al. Functional connectivity mapping for rTMS target selection in depression. Am J Psychiatr 2023;180:230–40. 10.1176/appi.ajp.20220306. [PubMed: 36855880]

[31]. Fox MD, Buckner RL, White MP, Greicius MD, Pascual-Leone A. Efficacy of transcranial magnetic stimulation targets for depression is related to intrinsic functional connectivity with the subgenual cingulate. Biol Psychiatry 2012;72:595–603. 10.1016/j.biopsych.2012.04.028. [PubMed: 22658708]

[32]. Cash RFH, Zalesky A, Thomson RH, Tian Y, Cocchi L, Fitzgerald PB. Subgenual functional connectivity predicts antidepressant treatment response to transcranial magnetic stimulation: independent validation and evaluation of personalization. Biol Psychiatry 2019;86:e5–7. 10.1016/j.biopsych.2018.12.002. [PubMed: 30670304]

[33]. Williams LM, Coman JT, Stetz PC, Walker NC, Kozel FA, George MS, et al. Identifying response and predictive biomarkers for Transcranial magnetic stimulation outcomes: protocol and rationale for a mechanistic study of functional neuroimaging and behavioral biomarkers in veterans with Pharmacoresistant depression. BMC Psychiatry 2021;21:35. 10.1186/s12888-020-03030-z. [PubMed: 33435926]

[34]. Madore MR, Kozel FA, Williams LM, Green LC, George MS, Holtzheimer PE, et al. Prefrontal transcranial magnetic stimulation for depression in US military veterans – a naturalistic cohort study in the veterans health administration. J Affect Disord 2022;297:671–8. 10.1016/j.jad.2021.10.025. [PubMed: 34687780]

[35]. Tozzi L, Bertrand C, Hack LM, Lyons T, Olmsted AM, Rajasekharan D, et al. A cognitive neural circuit biotype of depression showing functional and behavioral improvement after transcranial magnetic stimulation in the B-SMART-fMRI trial. Nat Ment Health 2024. 10.1038/s44220-024-00271-9.

[36]. Beam W, Borckardt JJ. https://clinicalresearcher.org/F3/2010.

[37]. Esteban O, Markiewicz CJ, Blair RW, Moodie CA, Isik AI, Erramuzpe A, et al. fMRIPrep: a robust preprocessing pipeline for functional MRI. Nat Methods 2019;16:111–6. 10.1038/s41592-018-0235-4. [PubMed: 30532080]

[38]. Mehta K, Salo T, Madison TJ, Adebimpe A, Bassett DS, Bertolero M, et al. XCP-D: a robust pipeline for the post-processing of fMRI data. Imaging Neurosci 2024;2:1–26. 10.1162/imag_a_00257.

[39]. Goldstein-Piekarski AN, Ball TM, Samara Z, Staveland BR, Keller AS, Fleming SL, et al. Mapping neural circuit biotypes to symptoms and behavioral dimensions of depression and anxiety. Biol Psychiatry 2022;91:561–71. 10.1016/j.biopsych.2021.06.024. [PubMed: 34482948]

[40]. Yarkoni T, Poldrack RA, Nichols TE, Van Essen DC, Wager TD. Large-scale automated synthesis of human functional neuroimaging data. Nat Methods 2011;8:665–70. 10.1038/nmeth.1635. [PubMed: 21706013]

[41]. Rush AJ, Trivedi MH, Ibrahim HM, Carmody TJ, Arnow B, Klein DN, et al. The 16-Item quick inventory of depressive symptomatology (QIDS), clinician rating (QIDS-C), and self-report (QIDS-SR): a psychometric evaluation in patients with chronic major depression. Biol Psychiatry 2003;54:573–83. 10.1016/S0006-3223(02)01866-8. [PubMed: 12946886]

[42]. Dale AM, Fischl B, Sereno MI. Cortical surface-based analysis: I. Segmentation and surface reconstruction. Neuroimage 1999;9:179–94. 10.1006/nimg.1998.0395. [PubMed: 9931268]

[43]. Puonti O, Van Leemput K, Saturnino GB, Siebner HR, Madsen KH, Thielscher A. Accurate and robust whole-head segmentation from magnetic resonance images for individualized

head modeling. Neuroimage 2020;219:117044. 10.1016/j.neuroimage.2020.117044. [PubMed: 32534963]

[44]. Glasser MF, Coalson TS, Robinson EC, Hacker CD, Harwell J, Yacoub E, et al. A multi-modal parcellation of human cerebral cortex. Nature 2016;536:171–8. 10.1038/nature18933. [PubMed: 27437579]

[45]. Thielscher A, Antunes A, Saturnino GB. Field modeling for transcranial magnetic stimulation: a useful tool to understand the physiological effects of TMS?. 2015 37th annu. Int. Conf. IEEE eng. Med. Biol. Soc. EMBC. Milan: IEEE; 2015. p. 222–5. 10.1109/EMBC.2015.7318340.

[46]. Deng Z-D, Lisanby SH, Peterchev AV. Electric field depth–focality tradeoff in transcranial magnetic stimulation: simulation comparison of 50 coil designs. Brain Stimul 2013;6:1–13. 10.1016/j.brs.2012.02.005. [PubMed: 22483681]

[47]. Siddiqi SH, Kandala S, Hacker CD, Trapp NT, Leuthardt EC, Carter AR, et al. Individualized precision targeting of dorsal attention and default mode networks with rTMS in traumatic brain injury-associated depression. Sci Rep 2023;13:4052. 10.1038/s41598-022-21905-x. [PubMed: 36906616]

[48]. Yesavage JA, Fairchild JK, Mi Z, Biswas K, Davis-Karim A, Phibbs CS, et al. Effect of repetitive transcranial magnetic stimulation on treatment-resistant major depression in us veterans: a randomized clinical trial. JAMA Psychiatry 2018;75:884. 10.1001/jamapsychiatry.2018.1483. [PubMed: 29955803]

[49]. Berlim MT, Van Den Eynde F, Tovar-Perdomo S, Daskalakis ZJ. Response, remission and drop-out rates following high-frequency repetitive transcranial magnetic stimulation (rTMS) for treating major depression: a systematic review and meta-analysis of randomized, double-blind and sham-controlled trials. Psychol Med 2014;44:225–39. 10.1017/S0033291713000512. [PubMed: 23507264]

[50]. Lacroix A, Calvet B, Laplace B, Lannaud M, Plansont B, Guignandon S, et al. Predictors of clinical response after rTMS treatment of patients suffering from drug-resistant depression. Transl Psychiatry 2021;11:587. 10.1038/s41398-021-01555-9. [PubMed: 34782593]

[51]. Siddiqi SH, Philip NS. Hitting the target of image-guided psychiatry? Am J Psychiatr 2023;180:185–7. 10.1176/appi.ajp.20230015. [PubMed: 36855875]

[52]. Fitzgerald PB. Targeting repetitive transcranial magnetic stimulation in depression: do we really know what we are stimulating and how best to do it? Brain Stimul. 2021;14(3):730–6. 10.1016/j.brs.2021.04.018. May-Jun. [PubMed: 33940242]

[53]. Wang W, Eisenberg SR. A Three-Dimensional Finite Element Method for Computing Magnetically Induced Currents in Tissues. IEEE Trans. Magn 1994;30:5015–23. 10.1109/20.334289.

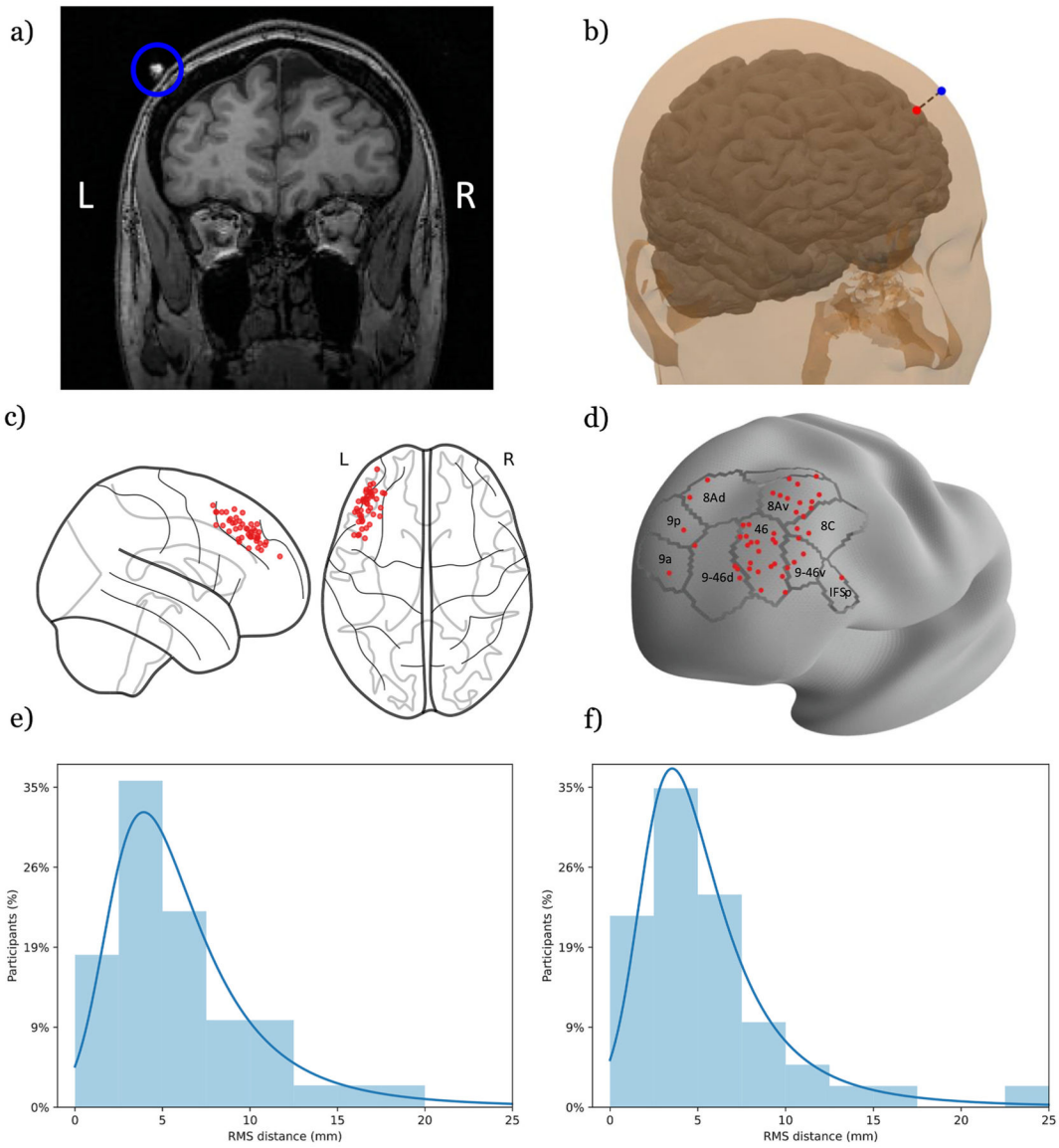

Fig. 1. The Beam/F3 method produces reliable TMS targets across individuals and repeated treatment sessions.

A high-contrast gel capsule (red circle) was used to visualize the Beam/F3 scalp target in structural MRI (a). Three-dimensional anatomical models of the scalp and cortical surfaces were reconstructed from segmented images; the Beam/F3 scalp target (blue dot) was projected orthogonally onto the cortex to derive a Beam/F3 cortical target (red dot) (b). For each participant, the Beam/F3 cortical target was registered to the MNI template (c) as well as the Glasser atlas (d). Using up to three separate imaging timepoints for each participant, the inter-session variability in stimulation targets was quantified as the RMS distance of individual session targets to the average target for both the Beam/F3 scalp target (e) and the projected cortical target (f). A noncentral *t*-distribution was fit to the data in (e) and (f). Abbreviations: RMS = root-mean-square. All two-dimensional image slices are displayed in neurological convention.

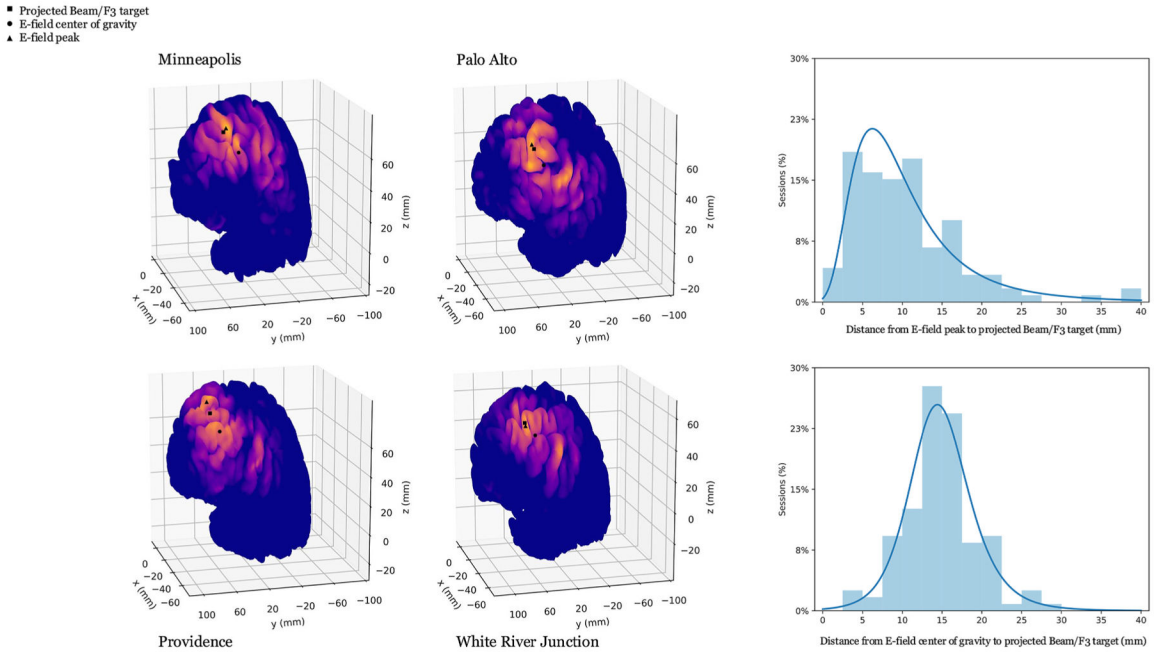

Fig. 2. Beam/F3 stimulation produces asymmetric electric fields, reflected by discordance between the Beam/F3 target and the E-field center of gravity.

Sample TMS E-fields induced by Beam/F3 coil placement at each VA hospital are shown on the left. Across participants, the peak of the E-field distribution (black triangle) was found at gyral crowns, typically located near the center of the TMS coil (black square; corresponding to the projected Beam/F3 target). E-fields preferentially propagated posteroinferiorly relative to the TMS coil center, such that the E-field center of gravity (black circle) typically occurred behind and below the Beam/F3 target. These observations were reflected in the distribution of the distance separating 1) the coil center and the E-field peak (top right) and 2) the coil center and the E-field center of gravity (bottom right) across TMS sessions. A non-central *t*-distribution was fit to these data. *Abbreviations*: E-field = electric field.

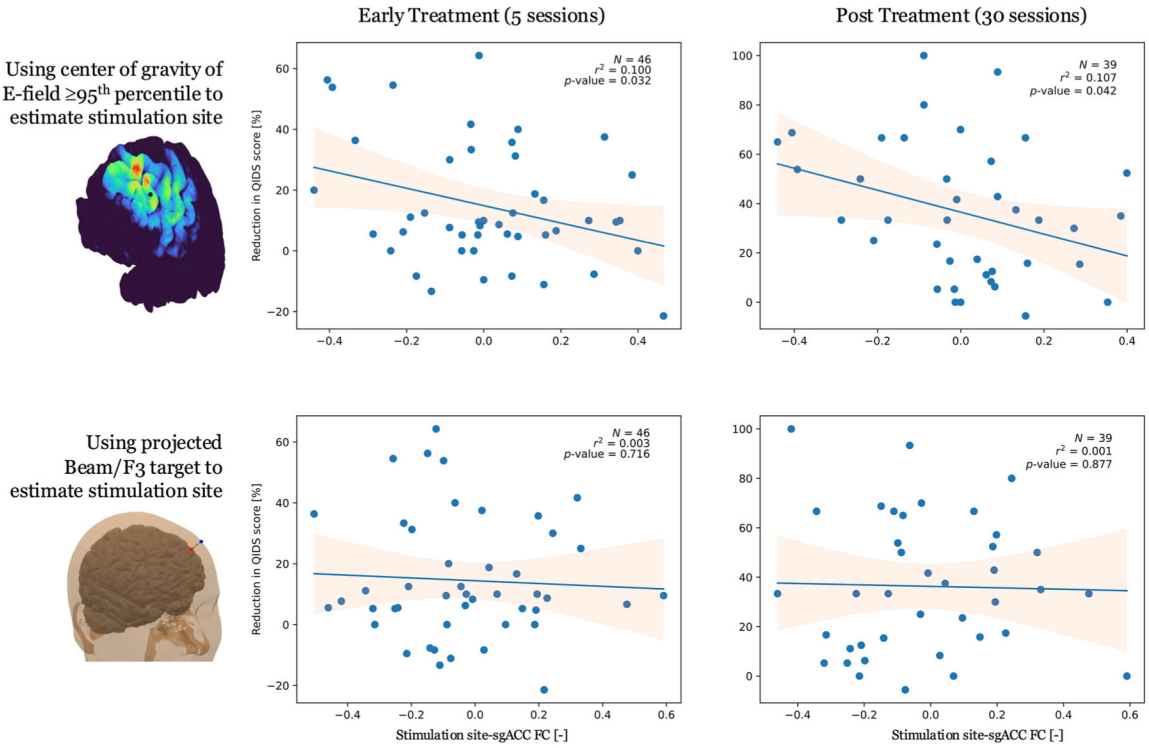

Fig. 3. Anticorrelation between the electric field center of gravity and the subgenual anterior cingulate cortex is associated with early and post-treatment depressive symptom reduction.

Stronger anticorrelation between the sgACC and the stimulation site, identified as the center of gravity of ≥95th percentile of the simulated electric field, was associated with improved symptom response both early in treatment (top left; $p = 0.032$, $r^2 = 0.100$, $N = 46$) and post treatment (top right; $p = 0.042$, $r^2 = 0.107$, $N = 39$). When the projected Beam/F3 cortical target was used as a first-order estimate of the stimulation site (i.e., without electric field data), no significant associations between sgACC anticorrelation and treatment response were observed either early in treatment (bottom left; $p = 0.716$, $r^2 = 0.003$, $N = 46$) or post treatment (bottom right; $p = 0.877$, $r^2 = 0.001$, $N = 39$). Abbreviations: E-field = electric field, FC = functional connectivity, sgACC = subgenual anterior cingulate cortex, QIDS = Quick Inventory of Depressive Symptomology.

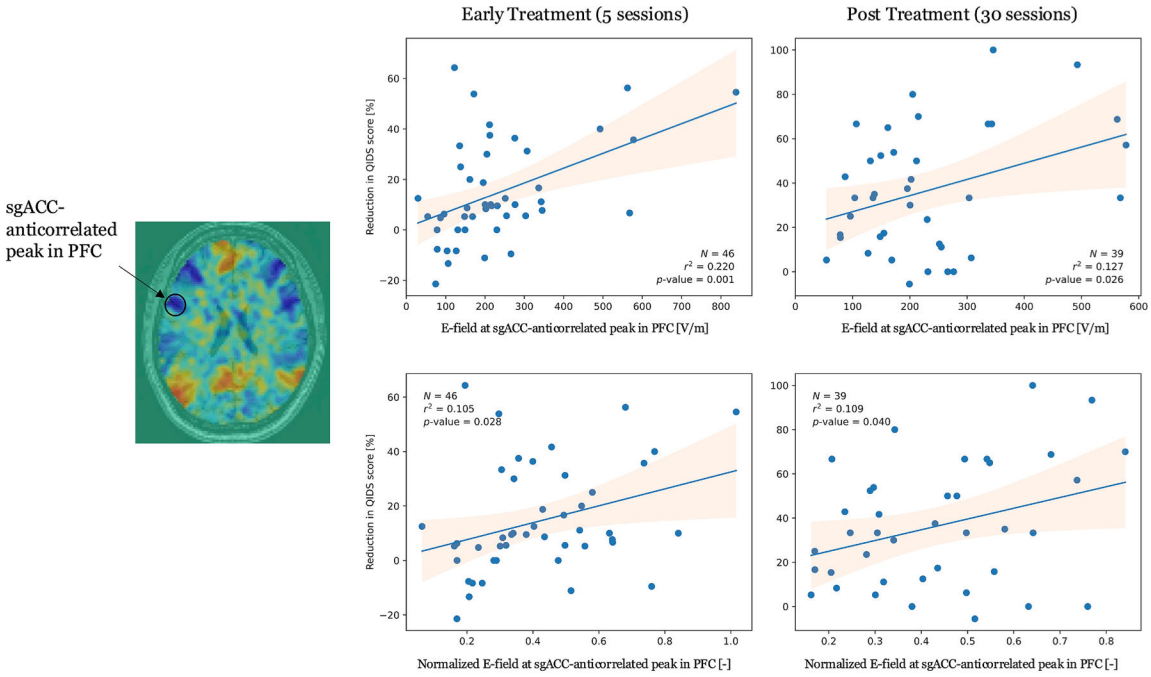

Fig. 4. TMS electric field magnitudes at the prefrontal sgACC-anticorrelated peak correlate with early and post-treatment depressive symptom reduction.

Higher E-field magnitudes at the peak sgACC-anticorrelated voxel in the prefrontal cortex was associated with greater depressive symptom reduction early in treatment (top left; $p = 0.001$, $r^2 = 0.220$, $N = 46$) and post treatment (top right; $p = 0.026$, $r^2 = 0.127$, $N = 39$). When the E-field at the sgACC-anticorrelated peak was normalized relative to the peak E-field induced on the cortex for each subject, this relationship remained significant both early in treatment (bottom left; $p = 0.028$, $r^2 = 0.105$, $N = 46$) and post treatment (bottom right; $p = 0.040$, $r^2 = 0.109$, $N = 39$). Abbreviations: E-field = electric field, sgACC = subgenual anterior cingulate cortex, PFC = prefrontal cortex, QIDS = Quick Inventory of Depressive Symptomology.

Table 1

Veteran sample characteristics. Abbreviations: SD = standard deviation, GED = General Educational Development Test, PTSD = post-traumatic stress disorder, ADHD = attention-deficit/hyperactivity disorder.

Age, *mean* ± *SD*	**47.39 ± 13.19**	***N* = 46**
Race, *n (%)*	White	41 (89%)
	Black	2 (4%)
	Asian	1 (2%)
	Other	2 (4%)
Ethnicity, *n (%)*	Hispanic	4 (9%)
	Not Hispanic	41 (89%)
	Decline to answer	1 (2%)
Gender, *n (%)*	Male	39 (85%)
	Female	7 (15%)
Highest Education, *n (%)*	High School/GED	5 (11%)
	Some college	10 (22%)
	Associate degree, vocational, or certificate program	10 (22%)
	Bachelor's degree	14 (30%)
	Master' s degree	7 (15%)
Treatment center, *n (%)*	Palo Alto	3 (7%)
	Providence	20 (43%)
	Minnesota	16 (35%)
	White River Junction	7 (15%)
Diagnosis, *n (%)*	PTSD	31 (67%)
	Substance Use Disorder	6 (13%)
	Alcohol Use Disorder	10 (22%)
	Anxiety Disorders	18 (39%)
	Obsessive Compulsive Disorder	4 (9%)
	ADHD	9 (20%)
	Personality Disorder	3 (7%)
	Other	1 (2%)